ACTIVE NOISE AND VIBRATION CONTROL SYSTEM DESIGN CONSIDERATIONS

Colin H. HANSEN[1], Xiaojun QIU[2], Cornelis PETERSEN[1], Carl HOWARD[1] and Sarabjeet SINGH[1]
[1]School of Mechanical Engineering
University of Adelaide
Adelaide, Australia, colin.hansen@adelaide.edu.au
[2]The Institute of Acoustics
Nanjing University
Nanjing, China, xjqiu@nju.edu.cn

Keywords: active noise control

1. Introduction

When designing active control systems to reduce structural vibration, to reduce sound transmission in ducts, to reduce vibration transmission through isolation systems or to reduce noise radiated by vibrating surfaces, there are many variables associated with the physical system arrangement that need to be optimised to achieve the maximum possible system performance. There are also a number of hardware and software aspects associated with the electronic controller that must be considered and accounted for when a laboratory system is adapted for operation in an industrial or commercial environment. There needs to be some sort of hierarchy in the approach to optimising the many variables which include type, locations and numbers of control sources, quality of the reference signal for feedforward systems, type, locations and numbers of error sensors, software structure and algorithm considerations and hardware architecture considerations. Control system software variables include convergence step size, number of filter taps for control and cancellation path filters, gain settings for both error signals in and control signals out, convergence coefficient and leakage coefficient size, control filter type, cancellation path model filter type and control algorithm. Control system hardware variables include type and accuracy of the A/D converter and general control system architecture. This paper will discuss a number of issues associated with the implementation of active noise and vibration systems that have been the subject of investigation at The University of Adelaide.

As mentioned above, the design of a practical active noise or vibration control system involves many choices and it is often difficult to make the correct choices unless the design of a system is approached in a systematic manner. This is why it is extremely difficult for a general purpose active noise control system to be optimal for any practical application as each application will be characterised by a different optimum set of choices. The order in which choices should be made and the different aspects that should be considered in the optimisation process was discussed in a previous paper [1] and has been slightly modified here (see Figure 1) to reflect recent advances made in cost function alternatives.

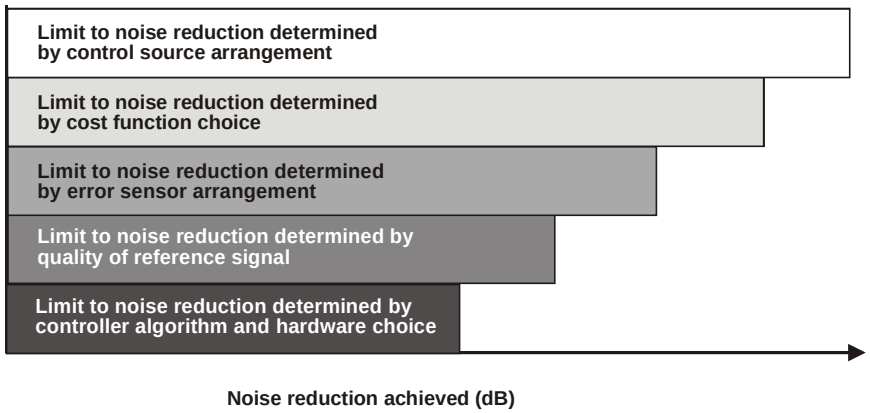

Figure 1. Hierarchy of active noise and vibration control system design.

For industrially based controllers, an additional consideration may be added at the bottom of the figure and that is the effect of an industrial environment on the overall performance of the control system, Things that need to be taken into account include the existence of transient events which could affect the stability of the controller, the ability for continuous monitoring on-site in a control room as well as at a remote location, power failures, transducer failures and electronic component failures.

The first parameter that must be optimised is the control source arrangement (number and location), as this will determine the maximum amount of cost function control achievable with an ideal error sensor arrangement and an ideal electronic controller. The control sources may be optimally arranged by using a genetic algorithm to determine the arrangement that minimises the specified cost function, which could be any one of a number of quantities including radiated sound power, global average sound pressure, energy density, pressure at one or more locations or structural vibration measures such as space averaged surface velocity.

The next parameter to be optimised is the choice of cost function that is to be minimised by the controller. This cost function is not necessarily the same as the cost function used to determine the optimum control source arrangement. For example, it may be the goal for the ANC system to minimise radiated sound power and this would be the cost function used in an analytical model and genetic algorithm to determine the optimum control source arrangement. However, it is often not possible to sense an ideal cost function such as sound power and an optimal alternative cost function has to be substituted. As

another example, the cost function to be minimised may be the sound pressure at a person's ear location and this ear location may also be continually moving. In this case, it is not practical to put a microphone in the person's ear and virtual sensing may be the optimal cost function. This would allow fixed microphones to be used to minimise the sound field at a moving location. Generally, the final choice of cost function will depend on many things, including the inconvenience or otherwise of implementing the required sensors and the susceptibility of the sensors to extraneous noise that is not part of the primary noise to be controlled.

The next parameter is the error sensor arrangement (number and locations), which will determine how close it will be possible to get with an ideal controller to the maximum achievable control set by the control source arrangement. For example, if microphones are used to measure a cost function based on minimising global average sound pressure levels, it can be shown that the optimal locations for them are where there is the greatest difference between the primary sound field and the theoretically optimally controlled field. This procedure, which involves the use of multiple regression, is discussed at length in Chapter 8 of Hansen and Snyder [2].

Next is the optimisation of the reference signal, which is needed for feedforward but not feedback systems. This generally means that if the controller is to reduce sound pressure levels or radiated sound power, the reference signal should be obtained by non-acoustic means if possible (such as with a tachometer) and if a microphone is used, care must be exercised to ensure that the reference signal is not influenced by flow noise or by the control signal. These considerations are discussed in detail by Hansen and Snyder [2].

The one remaining aspect not yet considered is the design of the electronic controller and this includes the software and hardware. For gradient descent algorithms to be effective in optimising the control filter weights (for FIR or IIR filters) and to minimise extraneous unwanted noise being introduced into the system through the control sources, it is necessary that the reference signal be well correlated with the error signals and with the sound to be minimised.

The remainder of this paper will discuss how these various aspects must be taken into account in active noise and vibration control system design. Attention will be focussed on aspects that were not discussed in a previous paper [1]. In particular, this paper will focus on some novel cost functions for active and semi-active noise control and a novel approach to controller software design for either active noise control or active vibration control.

2. Novel cost functions

In this section two novel cost functions will be discussed. The first is associated with a semi-active Helmholtz resonator system for controlling sound propagation in a duct and the second is associated with a virtual sensing system for local active noise control at a specified location which may be stationary or moving.

2.1. Development of a cost function for an adaptive Helmholtz resonator for a duct

An adaptive Helmholtz resonator is a convenient device that can be attached to the wall of a duct to minimise the transmitted sound power of a tonal noise having a wavelength that varies with time. The wavelength variation could be a result of variable

source operational conditions and/or varying temperatures in the duct. Such a system is defined as semi-active as the resonator is not generating any acoustic energy itself and control of the harmonic sound propagation is achieved by changing the resonator geometry. The minimisation of sound power is achieved by the resonator generating an impedance discontinuity that reflects the energy back upstream or suppresses its generation at the source. The ideal cost function in this case would be a direct measurement of transmitted sound power. Although it is possible to directly measure the sound power associated with plane waves propagating down the duct by using two microphones mounted in the duct wall at least one wavelength downstream of the resonator, it would be more useful if it were possible to obtain a measure of the transmitted power using microphones embedded in the resonator. In the latter case, the resonator could be a completely self-contained unit.

Unfortunately it can be shown that the minimum sound power transmission condition does not correspond to a maximum or minimum sound pressure anywhere in the resonator, nor does it correspond to a maximum or minimum in the transfer function between the sound pressure in the resonator neck and the sound pressure in the resonator cavity and nor does it correspond to a fixed value of the phase of the same transfer function. It was found that the relationship between minimum sound power transmission and the phase of the transfer function between the sound pressures in the resonator
neck and resonator cavity was dependent on the damping (reciprocal of the quality factor) in the resonator duct system. To find the value of the quality factor, the control system drives the piston, which forms the upper end of the resonator cavity, up and down until it finds a maximum of the ratio of the pressure in the resonator cavity (location A in Figure 2) to the pressure in the resonator neck (location B in Figure 2), as shown in [3]. The quality factor is then equal to this maximum value as shown in Figure 3. The vertical line corresponding to a cavity length of 70 mm corresponds to the minimum transmitted sound power. Once the quality factor is determined, the optimal phase difference of the transfer function may be determined by using a figure similar to Figure 4, which is for a specific family of resonators. The control system then drives the piston that changes the cavity volume until the required transfer function phase is achieved, thus minimising the transmitted power using only microphones mounted on the resonator.

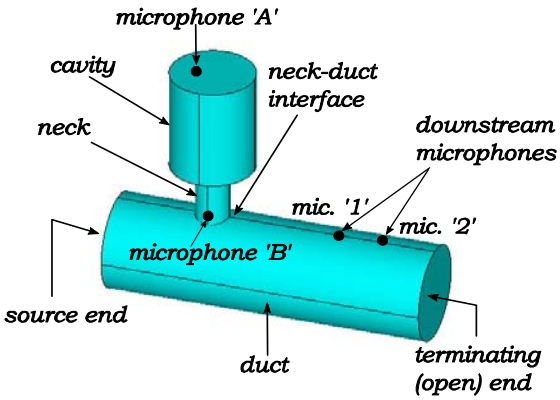

Figure 2. Helmholtz resonator set up.

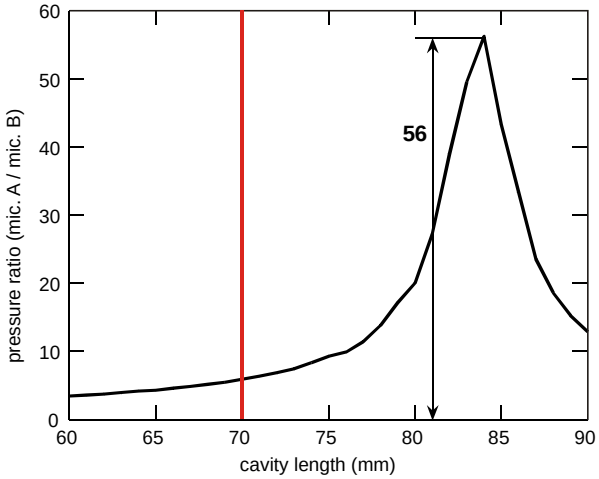

Figure 3. An example of determination of the maximum transfer function between the pressure at microphones A and B as a function of the resonator cavity length [3]. In this case the quality factor is 56.

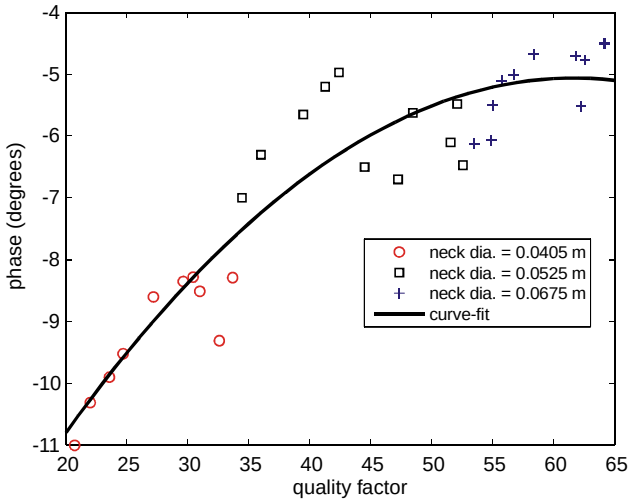

Figure 4. Transfer function optimal phase as a function of the measured quality factor of the duct/resonator system.

2.2. Virtual sensing cost functions for local active noise control

2.2.1. Background

In local active noise control, the cost function that is most commonly minimised is the mean-square pressure measured by an error microphone. This generally results in a zone of quiet that is centred at the physical location of the error microphone. For a pure

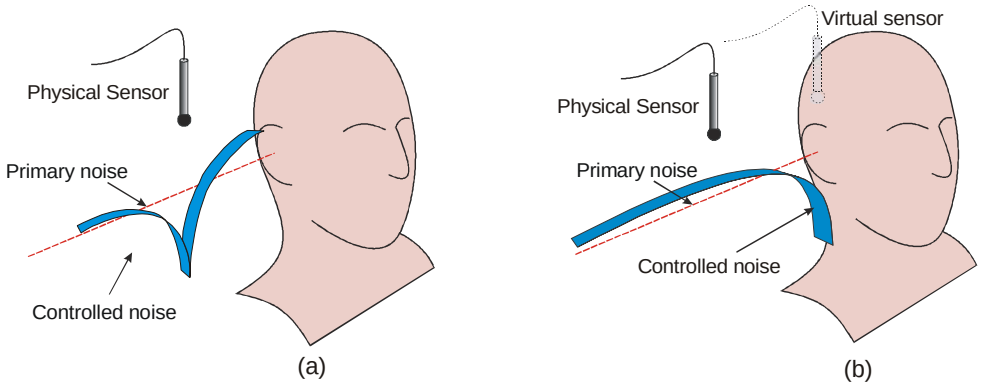

Figure 5. Local ANC (a) at a *physical* microphone and (b) at a *virtual* microphone.

tone diffuse sound field, it has been shown that the size of the created local zone of quiet, in which the noise is reduced by 10dB or more, is about one-tenth of an acoustic wavelength [4]. If the observer is to experience a significant attenuation in the noise, the error microphone thus has to be located relatively close to the observer's ear, which is not always an optimal or even possible solution. This problem is illustrated in Figure 5(a), where the term *physical sensor* denotes an error microphone that is physically measuring the pressure at a location in the sound field. Although a significant attenuation of the primary noise is obtained at the physical microphone in Figure 5(a), the zone of quiet is too small to extend to the observer's ear, such that the observer only experiences a small attenuation, or even amplification, in the primary noise.

To overcome the problem illustrated in Figure 5(a), *virtual sensing* methods for local active noise control systems have been suggested [5-9]. The principle of these methods is illustrated in Figure 5(b), where a *virtual microphone* has been located at the observer's ear where the maximum attenuation is required. Using the pressure measured by the physical microphone, the virtual sensing algorithm computes an *estimate* of the pressure at this virtual microphone. The cost function that is then minimised is the mean-square value of this estimated virtual pressure, instead of the mean-square pressure measured by the physical microphone. As illustrated in Figure 5(b), this results in a zone of quiet that is moved away from the physical microphone towards the location where the maximum attenuation is required, i.e. the *virtual location*.

2.2.2. Virtual sensing algorithms

The first virtual sensing algorithm that was suggested is called the *virtual microphone arrangement* [5]. In this algorithm, models of the secondary transfer paths between the control loudspeaker and the physical and virtual microphones are estimated in a preliminary identification stage in which a physical microphone is temporarily located at the virtual location. Furthermore, it is assumed that the primary pressures at the physical and virtual microphones are equal. This assumption and the secondary transfer path models are then used to compute an estimate of the virtual pressure given the pressure measured by the physical microphone and the control signal that excites the control loudspeaker. In another virtual sensing algorithm called the *remote microphone technique* [6,7], an additional filter is used which computes an estimate of the primary pressure at the virtual microphone given the primary pressure at the physical microphone. This filter is assumed to be unity in the virtual microphone arrangement [5], and this algorithm is therefore a simplified version of the remote microphone technique.

In another virtual sensing method, called the *adaptive LMS virtual microphone technique* [8], an array of physical microphones is used to compute an estimate of the virtual pressure. This estimate is computed as a weighted summation of the pressures measured by the physical microphone array. The weights are determined in a preliminary identification stage in which a physical microphone is temporarily located at the virtual location. The LMS algorithm [9] is then used to adapt the weights such that the difference between the pressure measured at the virtual location and the estimate of the virtual pressure is minimised. After convergence of the weights, the physical microphone temporarily located at the virtual location is removed, such that a virtual microphone is effectively created.

A virtual sensing method based on *Kalman filtering* has also been suggested [10]. This method uses one state-space model to describe the whole active noise control system, rather than a number of transfer path models. The pressure measured by the physical microphone is then used to compute a state-estimate given the state-space model of the active noise control system. This state-estimate is then used to compute an estimate of the virtual pressure. The state-space model of the active noise control system is estimated in a preliminary identification stage using *subspace model identification techniques* [11].

2.2.3. Number and locations of control loudspeakers, and physical and virtual microphones

Since a *local* active noise control system is considered here, the number and locations of the virtual microphones are of course determined by the desired locations of maximum attenuation, which are usually the ears of an observer. Physical microphones are initially located at the desired locations of maximum attenuation. The number of *control loudspeakers* and their locations are then selected to ensure that the control performance that is required at the virtual locations can be obtained with the chosen control loudspeaker configuration. Next, the pressures at the virtual locations are no longer directly measured by physical microphones, but estimated using a virtual sensing algorithm. At this stage, the number and locations of the *physical microphones* necessary to obtain an acceptable estimate of the sound pressure at the virtual locations are determined. Before defining what

is acceptable, it is important to understand how the estimation accuracy of the virtual sensing algorithm influences the control performance that can be obtained at the virtual locations. It has been shown that the attenuation that can be obtained when minimising an *estimate* of the pressures at the virtual locations is always smaller than or equal to the attenuation that can be obtained when minimising the *directly measured* pressures at these locations [12]. The difference in the obtained control performance is determined by how *accurately* the virtual sensing algorithm can estimate the *primary pressures* at the virtual microphones given the *primary pressures* at the physical microphones [5].

In one particular virtual sensing arrangement, called the virtual microphone arrangement [4], the control performance is limited by the validity of the assumption of equal primary pressures at the physical and virtual microphones.

Other virtual sensing arrangements [7,10] do not make the assumption of equal primary pressures at the physical and virtual microphones and in these cases, there are two factors that determine the estimation accuracy of the virtual sensing algorithms. The *first* factor that determines the estimation accuracy of the virtual sensing algorithm is related to observability. If there is noise that contributes to the primary pressures at the virtual microphones, but this noise is not measured, or observed, at the physical microphones, the virtual sensing algorithm is not able to estimate this part of the primary pressures at the virtual microphones. This is related to the concept of unobservable modes of the active noise control system [6], and is thus related to the locations of the physical and virtual microphones within the sound field. Thus, the number and locations of the physical microphones should be such that all the modes that contribute to the *primary pressures* at the virtual microphones are *observable* at the physical microphones.

The *second* factor that determines the estimation accuracy of the virtual sensing algorithm is related to the issue of *causality* that often arises in active noise control problems. Causality in the context of virtual sensing can be described as follows. If there is a *causal* relationship between the primary pressures at the physical and virtual microphones, the current value of the primary pressure at the virtual microphone only depends on the current and previous values of the pressure at the physical microphone. If there is a *non-causal* relationship, the current value of the primary pressure at the virtual microphone also depends on *future* values of the pressure at the physical microphone. Thus, the virtual sensing algorithm is only able to estimate those parts of the primary pressures at the virtual microphones that are *causally* related to the primary pressures at the physical microphones. The parts that are *non-causally* related cannot be estimated and therefore reduce the estimation accuracy of the virtual sensing algorithm. Thus, the number and locations of the physical microphones should be such that these causality issues are avoided as much as possible.

2.2.4. Moving virtual microphone

The virtual sensing methods discussed in Section 2.2.2 compute an estimate of the pressure at a virtual location that is *spatially fixed* within the sound field. In a practical situation, an observer will most likely move their head, and the desired location of maximum attenuation is thus generally *moving* through the sound field rather than being spatially fixed. This problem can be overcome by using a *moving virtual microphone* that tracks the desired location of maximum attenuation. An estimate of the pressure at this

moving virtual microphone can then be computed using a moving virtual sensing algorithm [7-9]. By minimising this estimate with an adaptive algorithm, a *moving zone of quiet* can be created that tracks the desired location of maximum attenuation, i.e. the *moving virtual location*. This concept has been experimentally demonstrated for narrowband noise inside an acoustic duct [7-9]. A schematic diagram of the rigidly terminated rectangular acoustic duct arrangement used in these experiments is shown in Figure 12.

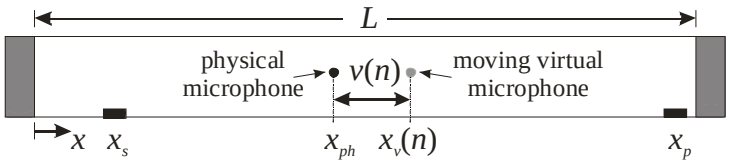

Figure 6. Schematic diagram of the rigidly terminated acoustic duct arrangement.

The acoustic duct arrangement shown in Figure 6 is of length L=4.83m, and has a primary loudspeaker located at x_p=4.73m, a control loudspeaker at x_s=0.1m, a physical microphone at x_{ph}=1.47m, and a *spatially fixed* virtual microphone at x_v=1.49m, which has not been shown in Figure 6. A *moving virtual microphone* is also located inside the duct, which tracks the desired moving location of maximum attenuation $x_v(n)= x_{ph}+v(n)$, with v the distance between the moving virtual microphone and the physical microphone, as illustrated in Figure 6. The primary loudspeaker is excited by a tonal signal of frequency 249Hz. A traversing microphone is used to measure the attenuation that is obtained at the moving virtual location $x_v(n)$. A typical result of the described experiment is shown in Figure 7.

The desired location of maximum attenuation $v(n)$ has been plotted against time in the bottom half of Figure 7. The moving virtual microphone is thus making a sinusoidal movement between a distance of 0.02m and 0.12m away from the physical microphone located at x_{ph}=1.47m, with a period of 5s. The attenuation measured at $v(n)$ with the traversing microphone has been plotted against time in the top-half of Figure 13, where the black line indicates the attenuation obtained while minimising the estimate of the pressure at the *spatially fixed* virtual microphone, and the grey line indicates the attenuation obtained while minimising the estimate of the pressure at the *moving* virtual microphone. The estimate of the pressure at the spatially fixed virtual microphone located at *v=0.02*m is computed using the virtual sensing algorithm introduced in [10]. The estimate of the pressure at the moving virtual microphone is computed using a Kalman filter based moving virtual sensing algorithm that is introduced in [16]. The minimisation of these estimates is performed using the filtered-x RLS algorithm as described in [16].

The results in Figure 7 show that when the desired location of maximum attenuation $v(n)$ is moving away from the virtual microphone *spatially fixed* at *v=0.02*m, the attenuation reduces drastically from 42dB to 15dB when minimising the estimate of the pressure at this spatially fixed virtual microphone. When the estimate of the pressure at the *moving virtual microphone* is minimised, the attenuation at the desired location of the zone of quiet $v(n)$ is relatively constant over time, and does not fall below 38dB. This indicates that a moving zone of quiet that tracks the desired location of maximum attenuation has effectively been

created inside the acoustic duct. The experimental results shown in Figure 7 therefore illustrate the increased control performance that can potentially be obtained in local active noise control systems when using a moving virtual sensing method instead of a spatially fixed virtual sensing method.

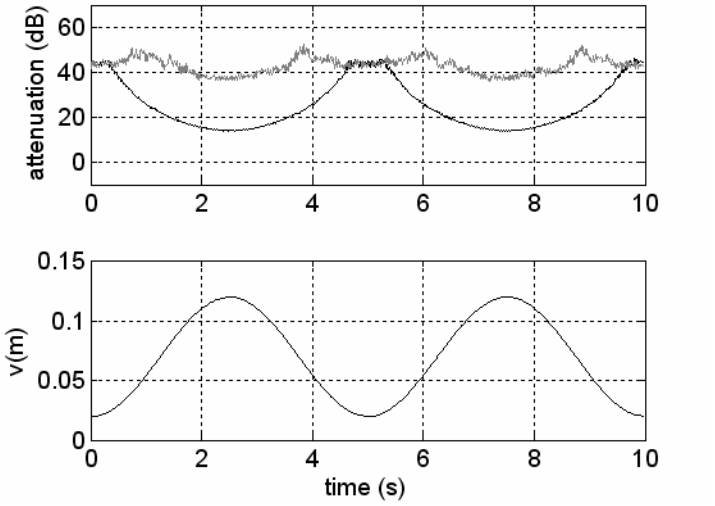

Figure 7. (*Top*) Attenuation obtained at the desired location of the zone of quiet $v(n)$ plotted against time, where the black line indicates minimising the estimate of the pressure at the *spatially fixed* virtual microphone located at $v=0.02$m, and the grey indicates minimising the estimate of the pressure at the *moving* virtual microphone that tracks $v(n)$. (*Bottom*) Desired location of the zone of quiet $v(n)$ plotted against time, with v the distance between the moving virtual microphone and the physical microphone located at x_{ph}=1.47m.

2.2.5. Increasing the zone of quiet around a virtual microphone

Instead of creating a moving virtual microphone that tracks the desired location of the zone of quiet, another approach is to try to *enlarge* the zone of quiet around a spatially fixed virtual location. This approach could for instance be used when the observer's ear is only making relatively small movements around a central spatially fixed position. In this case, the approach is thus to first move the zone of quiet away from the physical microphone to this central position, and to next enlarge the zone of quiet around this position. The enlargement of the zone of quiet can be achieved using two different approaches.

The *first* approach is to minimise estimates of the *pressure* and *pressure gradient* at the central spatially fixed virtual location, instead of only the pressure. It has been shown that the active cancellation of both pressure and pressure gradient along a single axis in a pure tone diffuse sound field using two secondary sources results in a zone of quiet that has the shape of a cylinder with rounded ends, with a length of about half an acoustic wavelength along the axis of the controlled pressure gradient, and a diameter of about one-

tenth of an acoustic wavelength [17]. If only pressure is minimised, the shape of the zone of quiet is expected to be a sphere with a diameter of about one-tenth of an acoustic wavelength [4]. Minimising *estimates* of both the pressure and pressure gradient thus has the potential to increase the size of the zone of quiet created around a spatially fixed virtual location [18].

The *second* approach is to estimate the pressures at a number of spatially fixed virtual microphones located at and around the central spatially fixed virtual location of interest. Minimising the sum of the mean-square values of these estimated pressures is then expected to enlarge the zone of quiet around the central position. This approach has been tested in the acoustic duct arrangement shown in Figure 6, where the primary loudspeaker is now excited by broadband noise in the frequency range of 50-500Hz. The physical microphone located at x_{ph}=1.47m is used in the virtual sensing algorithm introduced in [10] to compute an estimate of the pressures at five spatially fixed virtual microphones located at v=0.04, 0.06, 0.08, 0.10 and 0.12m. In the first experiment, only the estimated pressure at the central spatially fixed virtual microphone located at v=0.08m is minimised. In the second experiment, all of the five estimated pressures are minimised simultaneously. Figure 8 shows the resulting primary and controlled sound pressure distributions inside the acoustic duct arrangement, which have been measured using the traversing microphone. The dash-dotted line indicates the primary sound pressure distribution, the grey line the controlled sound pressure distribution obtained in the first experiment, and the black line the controlled sound pressure distribution obtained in the second experiment.

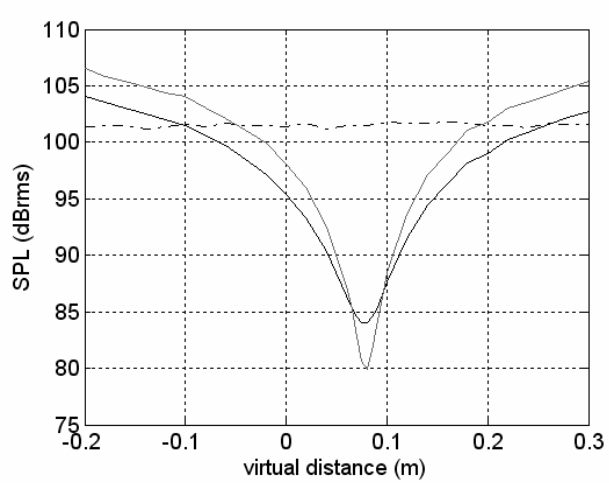

Figure 8. Moving and enlarging the zone of quiet using multiple spatially fixed virtual microphones and one physical microphone at v=0m. The dash-dotted line indicates the primary sound pressure distribution, the grey line the controlled sound pressure distribution obtained in the first experiment, and the black line the controlled sound pressure distribution obtained in the second experiment.

The results shown in Figure 8 show that in the first experiment, the zone of quiet has effectively been moved away from the physical microphone located at v=0m towards the central spatially fixed virtual microphone located at v=0.08m. In the second experiment, the zone of quiet has effectively been moved away to the central virtual location v=0.08m as well, but is now also enlarged. However, the enlargement of the zone of quiet results in 4dB less attenuation at the central virtual location of interest. This trade-off between enlarging the zone of quiet and the reduction in the peak attenuation that is obtained at the centre of the zone of quiet is also observed when minimising the estimated pressure and pressure gradient [17].

3. Software architecture and algorithm choice

When designing an active noise control system that will have as wide an application as possible, it is important to choose an algorithm and architecture that can cover a wide frequency bandwidth and at the same time be economical with computing resources. One such approach is discussed in the next section.

3.1. Multi-Rate Signal Processing and Sub-Band Filtering

Whenever the reference signal is available, a feedforward control system is often used due to its better control performance in terms of attenuation level and stability. To increase the upper limiting frequency and bandwidth of a feedforward control system, a higher system sampling rate often has to be used, and this brings a significant computational load, which precludes their use for many low-cost applications.

For example, consider a single channel active noise control system in a duct, where the impulse response from the control source to the error sensor is about 0.25s due to the reflections from the ends of the duct. If the noise to be controlled is below 500Hz, the sampling frequency can be 1000Hz, and the length of the FIR filter for modelling the cancellation path should be about 250 taps. However, if the noise components to be controlled are up to 5000Hz, then the sampling frequency needs to be 10000Hz, and the length of the cancellation path FIR filter should be about 2500 taps. For a typical DSP processor, usually 1 instruction cycle is needed for one tap FIR filtering operation and 2 instruction cycles are needed for one tap LMS update operation; thus at least 7500 instruction cycles are needed for the control filter update of the single channel ANC system which has the FXLMS algorithm implemented. If the system needs to be updated every sample, this requires the processing capability of the DSP processor be greater than 75MFLOPS, ten times higher than that of the system with 1000Hz sampling frequency.

A number of algorithms have been proposed to reduce the computation load of the FXLMS algorithm. For example, the block FXLMS algorithm uses the sum of the mean-square errors over a period of samples as its cost function, resulting in less frequent update on block by block basis; the periodic FXLMS algorithm reduces the computational load by updating the filter coefficients every N samples with the N^{th} samples, and the periodic block algorithm is a combination of the previous two, which updates the filter coefficients every N samples with a small block of data where the block size is much smaller than that of the block FXLMS algorithm, but larger than the number of samples in a period of the disturbance. The frequency domain algorithm can also be used, which involves

implementation of the control filtering in the time domain and updating of the control filter coefficients in the frequency domain.

With the above algorithms, the computation load can be substantially reduced, yet there are still some problems associated with each of them. For example, the periodic FXLMS algorithm may suffer from a long convergence time, and the implementation of the frequency domain algorithm may need large on-chip memory. There is another kind of time and frequency domain algorithm called the sub-band FXLMS algorithm, which uses multi-rate signal processing techniques. With this approach, the input signals from the reference and error sensors are sampled at a high frequency and filtered into many sub-bands. Each sub-band signal is then phase-shifted and down-sampled at a lower sampling rate and then processed to frequency shift it to a base band, which spans a frequency range from 0 Hz to an upper frequency that is dependent on the original sampling rate and the number of sub-bands used to divide up the frequency range of interest. For each sub-band, an adaptive control filter is used to provide the sub-band control signal, and the signals from each sub-band are combined and up-sampled to synthesize the full-band control signal. If each sub-band is characterised by different energy levels, then the control system performance can be optimised for maximum convergence speed in each sub-band by using a filtered-X normalised LMS (FXNLMS) algorithm where the convergence coefficient is normalised by the band signal power.

Applying multi-rate signal processing techniques in active noise control has several advantages. For example, the high sample rate sometimes can eliminate the need for sharp anti-aliasing filters and reduces the inherent one sample delay of the digital system. Each sub-band can have its own convergence coefficients and the signal dynamic range is greatly reduced in each sub-band, so the whole control system is likely to converge faster and track more quickly. However, the most important advantage is that the computation complexity for the control filter update can be greatly reduced by approximately the number of the sub-bands due to the reduced number of filter taps and weight update rate in each sub-band, and for narrow band noise, both the computation complexity and the memory requirement can be further reduced. As the sub-band FXLMS algorithm with a large number of sub-bands has more computation complexity reduction and processing flexibility in addition to the potential of a faster convergence speed, this paper will focus on the discussion of this algorithm.

The delayless sub-band adaptive architecture for the FXLMS algorithm was proposed in [19], where the signal path delay was avoided by updating the adaptive weights in sub-bands while carrying out the signal filtering in full-band with additional computation load resulting from transforming the sub-band coefficients to full-band, using the frequency stacking method. Several new schemes have been proposed to improve the performance of the sub-band-full-band weight transformation [20, 21]. Also, the sub-band cancellation path modeling and the sub-band filtered reference signal generation methods have also been proposed for the delayless sub-band adaptive architecture to further reduce the computation load [22]. The above delayless sub-band ANC algorithms were extended to multi-channel systems by Qiu et al. [23].

Sub-band filtering techniques have been widely used in the telecommunication field. However, the common sub-band structures used in adaptive echo cancellation introduce a delay in the signal path, which limits their implementation in active noise control. To eliminate the signal path delay, the adaptive weights can be updated in sub-bands while the

signal filtering is carried out in full-band with additional computation load resulting from transforming the sub-band coefficients to full-band. Figure 9 shows the structure of the single channel delayless sub-band ANC system with the physical cancellation path transfer function $C(z)$, which is modelled by injecting uncorrelated random noise $r(n)$ into the system. $x(n)$ is the reference signal from the noise source and $P(z)$ is the primary path transfer function between the primary noise $p(n)$ and $x(n)$. The output of the controller $W(z)$ is $y(n)$, and the error signal $e(n)$.

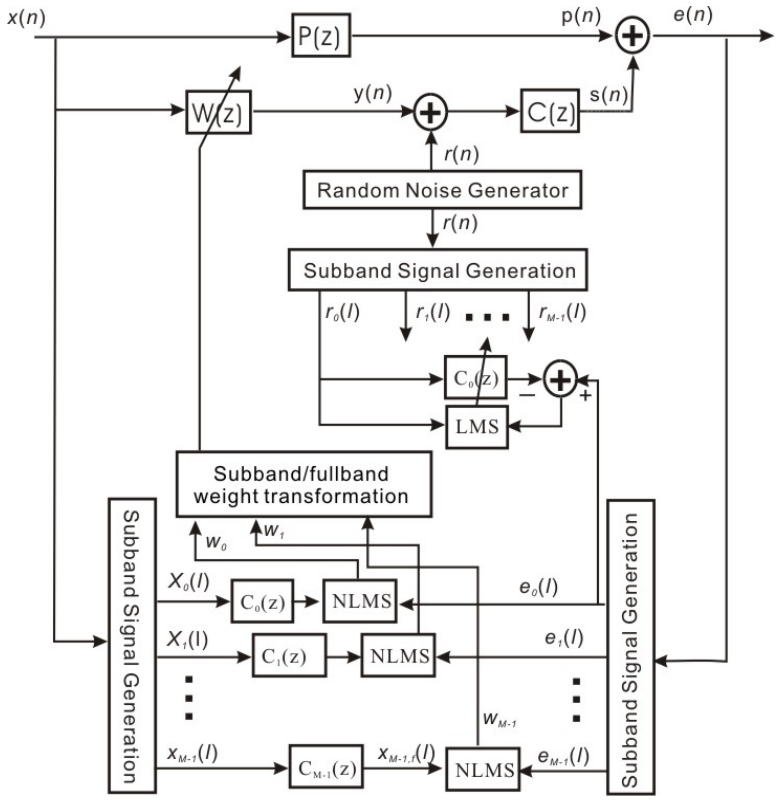

Figure 9. Delayless sub-band ANC system using the FXLMS algorithm

The system consists of 5 parts: sub-band signal generation; sub-band cancellation path modelling; sub-band adaptive weight update; sub-band/full-band weight transformation; and full-band control signal generation (control filtering). All of these are described below. The main difference between the sub-band algorithm and the common full-band FXLMS algorithm, is that, except for the control signal generation, which is carried out in full-band to avoid delay, all parts of the control system operate in each sub-band at a decimated sample rate. This reduces the computation load and allows independent and different convergence coefficients, thus allowing the controller to operate over a wider band-width. Note that the same sample rate is used on each sub-band, as frequency shifting

is carried out on each band before down sampling so that all bands are processed in the base band. In all of the following, it is possible to replace the FXLMS algorithm with the normalised. Thus, if each sub-band is characterised by different energy levels, then the control system performance can be optimised for maximum convergence speed in each sub-band by using a filtered-X normalised LMS (FXNLMS) algorithm where the convergence coefficient is normalised by the band signal power.

As an example consider a 16kHz sampling frequency and a frequency range of interest of 0 to 4000Hz. If the sample rate is down-sampled to 250Hz for the sub-bands, then this implies that there will be 64 sub bands (16000/250). The maximum frequency for each sub-band is half the sampling frequency; that is, 125Hz. As the upper frequency of interest is 4000Hz, only the first 32 sub-bands need to be processed (4000/125 = 32), which, for a 4000Hz band-width divided into 64 sub-bands, is 0-125Hz. Note that it is possible to over sample and still have the same number of sub-bands so that many more samples are taken for each cycle. In the current example, if we wished to sample at 10 times the upper frequency of the sub-band, we still could do that and have the same number of sub-bands. This would give better results at the lower end of each sub-band.

The procedure for generating the sub-band signals will now be discussed. The m^{th} sub-band signal, $x_m(l)$, is calculated by bandpass filtering, frequency shifting, and down sampling the full-band signal $x(n)$,

$$\begin{aligned} x_m(l) &= \sum_{k=0}^{K_L-1} a_k e^{-j2\pi\frac{mk}{M}} x(Dl-k) \\ &= \sum_{k=0}^{M-1} e^{-j2\pi\frac{mk}{M}} \sum_{n=0}^{K_L/M-1} a_{k+nM}\, x(Dl-k-nM) \end{aligned} \tag{1}$$

where l is the sub-band index, D is the down sampling frequency, a_k are the coefficients of a K_L point low pass prototype FIR filter and K_L usually is larger than the number of sub-bands M to avoid aliasing. The calculation complexity for all sub-band signal generation can be reduced by using the polyphase FFT method:

$$\begin{bmatrix} x_0(l) & x_1(l) & \cdots & x_{M-1}(l) \end{bmatrix}^T = FFT\{\mathbf{F}\mathbf{x}(l)\} \tag{2}$$

where the K_L point column vector, $\mathbf{x}(l) = [x(Dl)\ x(Dl\text{-}1)\ \cdots\ x(Dl\text{-}K_L\text{+}1)]^T$, the prototype filter matrix $\mathbf{F}$ is of size $M \times K_L$, and an example with $M = 4$ and $K_L = 8$ is shown below..

$$\mathbf{F} = \begin{bmatrix} a_0 & 0 & 0 & 0 & a_4 & 0 & 0 & 0 \\ 0 & a_1 & 0 & 0 & 0 & a_5 & 0 & 0 \\ 0 & 0 & a_2 & 0 & 0 & 0 & a_6 & 0 \\ 0 & 0 & 0 & a_3 & 0 & 0 & 0 & a_7 \end{bmatrix} \tag{3}$$

The D new input samples are shifted into $\mathbf{x}(l)$ and multiplied with the prototype filter matrix $\mathbf{F}$. The M sub-band signals are obtained by applying a FFT to the obtained M point product. In the algorithm shown in Figure 9, the reference signal, the error signal and the modelling signal are all decomposed into sub-band signals using this method. The

generated sub-band signals are complex values, so complex valued adaptive filters are needed. However, as the full-band signal and the prototype filter matrix are real values, it is only necessary to do the calculation for the first $M/2+1$ sub-bands.

Figure 9 also illustrates the method used to obtain the sub-band cancellation path transfer functions where the modelling signal $r(n)$ (random noise) is decomposed into M sub-band modelling signals, which are used with the M sub-band error to directly obtain the sub-band cancellation path transfer functions. The update equation for the sub-band FXLMS algorithm in each sub-band is almost the same as that of full-band FXLMS algorithm, except that complex valued filtering and the LMS algorithm have to be used.

The purpose of the sub-band/full-band filter weight transform is to transform a set of M sub-band filter weights $\mathbf{W}_m$ of length N_s, into a corresponding full-band filter $\mathbf{W}$ of length N. Several methods have been developed, such as the DFT stacking method, the DFT-2 stacking method, the DFT-FIR weight transform and the linear weight transform. For example, by using the DFT-FIR weight transform, the full-band filter weights are obtained by using the sub-band filter weights as input sub-band signals to the synthesis filters. The full-band signal (weights) can be obtained by summation of all the sub-band signals after up sampling, bandpass filtering and frequency shifting.

It should be noted that the maximum computation complexity reduction of the single channel delayless sub-band ANC system with the FXLMS algorithm is only about 33% of that of the full-band FXLMS algorithm due to the delayless requirement. However, the computation complexity reduction provided by the multi-channel delayless sub-band ANC system with the MFXLMS (multi-channel FXLMS) algorithm can be much more. The multi-channel sub-band ANC system consists of the same 5 parts as the single channel case: cancellation path modelling; adaptive weight updating; and sub-band/full-band weight transformation. These steps are all carried out in each sub-band at the reduced sampling frequency to reduce the computation load, and only multi-channel control signals are generated by full-band FIR filters to avoid delay. Figure 10 shows the ratio of the computation complexity of the sub-band MFXLMS to the full-band MFXLMS when

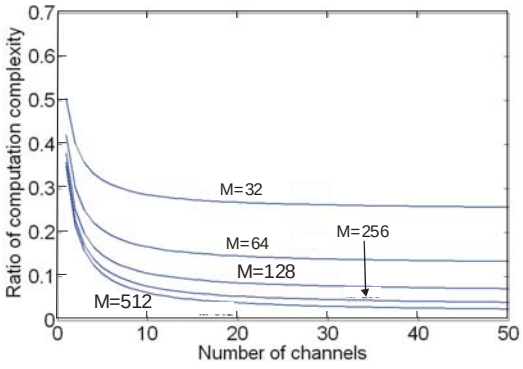

Figure 10. The ratio of the computation complexity of the sub-band to the full-band MFXLMS as a function of the number of the control channels for different numbers of sub-bands, M.

the sub-band number is 32, 64, 128, 256 and 512 as a function of the number of the control channels. In this case, the length of the control filter and cancellation path filter are 4096, with two times over sampling in the sub-bands ($D=M/2$). The length of the prototype filter is 4 times that of the sub-band number. It can be seen that with the increase of sub-band number, the computation load of the sub-band MFXLMS algorithm with a large number of channels can be reduced to about $8/M$ of that of the full-band. It can also be seen that when M is larger than a particular value, further increasing M cannot further reduce the computation load of the sub-band algorithm significantly, as the main contributor to the computation load becomes the control signal generation part at full-band.

Conclusions

The design of an effective and versatile active noise or vibration control system requires that many different aspects of the design be successfully addressed. Many of these aspects interact with one another so the order in which each is addressed and optimised is important. The team involved in a successful active noise or vibration control system development must have collective expertise in acoustics, vibration, signal processing, control theory and application, and digital electronic systems. All of this expertise is necessary in order to optimise the performance and stability of an active noise control system. Many of the issues that must be considered in optimising an active noise control system as well as the order in which they should be addressed have been discussed in this paper. In particular the paper focussed on novel cost functions and a wide bandwidth software architecture and algorithm.

References

[1] Hansen, C.H. “Active noise control - from laboratory to industrial implementation”, *Proceedings of Noise-Con '97*, Penn State Univ, June 15-17 1997, pp. 3-38.

[2] Hansen, C.H. and Snyder, S.D. *Active control of sound and vibration*. London: E&FN Spon, 1997.

[3] Singh, S., Hansen, C.H. and Howard, C.Q. “The elusive cost function for tuning adaptive Helmholtz resonators”, *Proceedings of the First Australasian Acoustical Societies' Conference*, November 20-22 2006, Christchurch, New Zealand.

[4] Elliott, S.J., Joseph, P., Bullmore, A.J. and Nelson, P.A. “Active cancellation at a point in a pure tone diffuse sound field.” *Journal of Sound and Vibration*, **120**, pp.183-189, (1988)

[5] Elliott, S.J. and David, A. “A virtual microphone arrangement for local active sound control”, *Proceedings of the 1st International Conference on Motion and Vibration Control*, Yokohama, 1992, pp.1027-1031.

[6] Roure, A. and Albarrazin, A. “The remote microphone technique for active noise control”, *Proceedings of Active '99*, Fort Lauderdale, USA, 1999, pp.1233-1244.

[7] Popovich, S.R. “Active acoustic control in remote regions.” US Patent No. 5,701,350, (1997)

[8] Cazzolato, B.S. “An adaptive LMS virtual microphone”, *Proceedings of Active '02*, ISVR, Southampton, UK, 2002, pp.105-116.

[9] Haykin, S., *Adaptive Filter Theory*, Prentice Hall, 2002.

[10] Petersen, C.D., Fraanje, R., Cazzolato, B.S., Zander, A.C. and Hansen, C.H. “A Kalman filter approach to virtual sensing for active noise control” submitted to *Mechanical Systems and Signal Processing*, (2006).
[11] Overschee van, P. and Moor de, B. *Subspace Identification for Linear Systems: Theory, Implementation, Applications*. Boston : Kluwer Academic Publishers, 1996.
[12] Petersen, C.D., Zander, A.C., Cazzolato, B.S., Fraanje, R. and Hansen, C.H. “Limits on active noise control performance at virtual error sensors.” *Proceedings of Active '06*, Adelaide, South Australia, 2006, pp. 1233-1244.
[13] Zhou, K., Doyle, J.C. and Glover, K. *Robust and Optimal Control*, Prentice-Hall, Inc. New York, 1996.
[14] Petersen, C.D., Zander, A.C., Cazzolato, B.S. and Hansen, C.H. “A moving zone of quiet for narrowband noise in a one-dimensional duct using virtual sensing.” *Journal of the Acoustical Society of America*, **121**, (2007).
[15] Petersen, C., Cazzolato, B., Zander, A. and Hansen, C. “Active noise control at a moving location using virtual sensing.” Proceedings of the Thirteenth International Congress on Sound and Vibration, Vienna, Austria, 2006.
[16] Petersen, C.D., “Virtual sensing for active noise control at a moving location”, Ph.D. Thesis, School of Mechanical Engineering, The University of Adelaide, 5005 SA, Australia, (2007).
[17] Elliott, S.J. and Garcia-Bonito, J., “Active cancellation of pressure and pressure gradient in a diffuse sound field.” *Journal of Sound and Vibration*, **186**, 696-704 (1995).
[18] Garcia-Bonito, J., Elliott, S.J. and Boucher, C.C. “A novel secondary source for a local active noise control system.” *Proceedings of Active '97*, Budapest, Hungary, 1997, pp. 405-418.
[19] Morgan, D.R. and Thi, J.C. “A delayless sub-band adaptive filter architecture”, *IEEE Trans. Signal Processing*, **43**, 1818-1830 (1995).
[20] Huo, J., Nordholm, S. and Zang, Z. “New weight transform schemes for delayless sub-band adaptive filtering”, *Proceedings of IEEE Global Telecommunications Conference*, 2001, pp.197-201.
[21] Larson, L., de Haan, M. and Claesson, I. “A new sub-band weight transform for delayless sub-band adaptive filtering structures”, *IEEE Digital Signal Processing Workshop* 2002, pp.201-206.
[22] Park, S.J., Yun, J.H. and Park, Y.C. “A delayless sub-band active noise control system for wideband noise control”, *IEEE Trans. Speech and Audio Processing*, **9**, 892-899 (2001).
[23] Qiu, X., Ningrong, L., Chen, G. and Hansen, C.H. “The implementation of delayless subband active noise control algorithms”, *Proceedings of Active '06*, September 18-20, Adelaide, Australia, 2006.